Correlating Carrier Type with Frontier Molecular Orbital Energy Levels in Organic Thin Film Transistors of Functionalized Acene Derivatives

Ming L. Tang,[†] Anna D. Reichardt,[†] Peng Wei,[‡] and Zhenan Bao*,[‡]

Departments of Chemistry and Chemical Engineering,
Stanford University, Stanford, California 94305

Received December 10, 2008; E-mail: zbao@stanford.edu

Abstract: We investigate the relationship between the charge carrier type in organic thin film transistors (OTFTs) and molecular energy levels. We examine a series of functionalized acenes that collectively have their HOMOs range from -4.9 eV to -5.6 eV and LUMOs range from -2.8 eV to -3.7 eV, as measured by cyclic voltammetry. Placed together, these 20 molecules allow us to chart the transition from OTFTs that display only hole transport, to ambipolar, to solely electron transport. Specifically, we note that for octadecyltrimethoxysilane (OTS) treated substrates, with top contact gold electrodes, electron injection and transport occurs when the LUMO < -3.15 eV, while hole injection and transport ceases when the HOMO < -5.6 eV. Ambipolar transport prevails when molecules have HOMO/LUMO levels within the aforementioned range. This is seen across channel lengths ranging from $50-150$ μm and using only gold as electrodes. This empirical plot is the first time such a detailed study has been made on the onset of charge injection and transport for a class of organic semiconductors. It provides guidelines for future molecular design.

Organic semiconductors offer the possibility of low-cost, solution-based processing for various electronic applications that do not require high switching speeds.[1,2] To enable organic semiconductors (OSCs) as the active components in large area displays, sensors or radio frequency identification (RFID) tags, a fundamental understanding of how OSC-based devices operate is required, whether as organic light-emitting diodes (OLEDs),[3−6] organic thin film transistors (OTFTs)[1,7−9] or organic photovoltaics (OPVs).[10,11]

Organic thin film transistor devices are attractive because of their potential to be flexible and transparent. However, since most organic semiconductor thin films are polycrystalline, it is difficult to deconvolute the effects of molecular structure, dielectric properties, grain boundaries, traps by ambient species, etc. from the measured OTFT mobility, on/off ratio and

threshold voltage, for example. It is nearly impossible to predict from first principles how a given material would perform as an OTFT in terms of mobility, although qualitatively one can predict its stability, solubility, charge carrier type, etc. In order to design electronic devices that incorporate organics, it is vital to know the charge carrier type of the active material. An OTFT is a good tool to measure the carrier type of the organic material, and to quantify its velocity per unit electric field in the plane of the substrate.

It is understood qualitatively that charge carrier type for a given molecule or polymer depends on its molecular energy levels.[12] Electron-withdrawing groups tend to lower the molecular orbital energy levels of organic semiconductors, allowing electron injection into the lowest unoccupied molecular orbital (LUMO), while the converse is true for hole transport, where holes tunnel into the highest occupied molecular orbital (HOMO) when the HOMO is in resonance with the workfunction of the electrodes. There is no intrinsic reason why OSCs should not transport both holes and electrons. Indeed, by varying the workfunction of the electrodes,[13] eliminating traps on oxide surfaces,[14] improving OSC purity and reducing structural defects, or by having molecules that possess a low bandgap[15,16] such that the barrier to injection of both charges is surmountable,

[†] Department of Chemistry.
[‡] Department of Chemical Engineering.

(1) Murphy, A. R.; Frechet, J. M. J. *Chem. Rev.* **2007**, *107*, 1066–1096.
(2) Bao, Z.; Locklin, J. *Organic Field-Effect Transistors (Optical Science and Engineering Series)*; 1st ed.; CRC Press: Boca Raton, FL, 2007.
(3) Shirota, Y.; Kageyama, H. *Chem. Rev.* **2007**, *107*, 953–1010.
(4) Walzer, K.; Maennig, B.; Pfeiffer, M.; Leo, K. *Chem. Rev.* **2007**, *107*, 1233–1271.
(5) Baldo, M. A.; Thompson, M. E.; Forrest, S. R. *Nature* **2000**, *403*, 750–753.
(6) Baldo, M. A.; O'Brien, D. F.; You, Y.; Shoustikov, A.; Sibley, S.; Thompson, M. E.; Forrest, S. R. *Nature* **1998**, *395*, 151–154.
(7) Anthony, J. E. *Chem. Rev.* **2006**, *106*, 5028–5048.
(8) Smits, E. C. P.; et al. *Nature* **2008**, *455*, 956–959.
(9) Halik, M.; Klauk, H.; Zschieschang, U.; Schmid, G.; Dehm, C.; Schutz, M.; Maisch, S.; Effenberger, F.; Brunnbauer, M.; Stellacci, F. *Nature* **2004**, *431*, 963–966.
(10) Blom, P. W. M.; Mihailetchi, V. D.; Koster, L. J. A.; Markov, D. E. *Adv. Mater.* **2007**, *19*, 1551–1566.
(11) Gunes, S.; Neugebauer, H.; Sariciftci, N. S. *Chem. Rev.* **2007**, *107*, 1324–1338.

(12) Newman, C. R.; Frisbie, C. D.; da Silva, D. A.; Bredas, J. L.; Ewbank, P. C.; Mann, K. R. *Chem. Mater.* **2004**, *16*, 4436–4451.
(13) Yasuda, T.; Goto, T.; Fujita, K.; Tsutsui, T. *Appl. Phys. Lett.* **2004**, *85*, 2098–2100.
(14) Chua, L. L.; Zaumseil, J.; Chang, J. F.; Ou, E. C. W.; Ho, P. K. H.; Sirringhaus, H.; Friend, R. H. *Nature* **2005**, *434*, 194–199.
(15) Zaumseil, J.; Sirringhaus, H. *Chem. Rev.* **2007**, *107*, 1296–1323.
(16) Smits, E. C. P.; Setayesh, S.; Anthopoulos, T. D.; Buechel, M.; Nijssen, W.; Coehoorn, R.; Blom, P. W. M.; de Boer, B.; de Leeuw, D. M. *Adv. Mater.* **2007**, *19*, 734–738.

ambipolar transport is observed. However, it is difficult to directly relate the HOMO/LUMO levels measured in solution to charge carrier type in thin film in a quantitative manner.

In this paper, we experimentally show the correlation between charge carrier type in the OTFT geometry and the molecular HOMO/LUMO levels measured by cyclic voltammetry in solution. This is enabled by a series of 19 molecules that have HOMOs ranging from −4.9 to −5.6 eV and LUMOs ranging from −2.8 to −3.7 eV. All these molecules are pentacene and tetraceno[2,3-*b*]thiophene based and thus have five linearly fused rings and are with or without the tri-isopropylsilylacetylene substitution at the central position. These molecules are in the same acene family, and allow for useful comparison. The most common device structure used in literature has gold electrodes (even for n-channel OSCs) and octadecylsilane (OTS)-treated silicon dioxide surfaces to passivate traps. We employed this common device structure in this study to investigate the transition from hole-only to ambipolar to electron-only OTFTs for these linear acenes.

Experimental Methods

Instrumentation. NMR (^{1}H and ^{13}C) spectra were recorded on a Varian Inova-500 MHz spectrometer at room temperature unless indicated otherwise. The ^{1}H and ^{13}C chemical shifts (δ) are reported in parts per million, and the residual solvent peak was used as an internal standard. The Philips PANalytical X'Pert diffractometer with a PreFIX X-ray mirror at the incident beam and a parallel plate collimator at the diffracted beam was used on the thin films of the evaporated molecules. $\omega/2\theta$ scans were performed with Cu Kα radiation at a power of 45 mV and 40 mA, with a step size of 0.02°, and a step time of 1.0 s. A Digital Instruments (DI) MMAFM-2 scanning probe microscope was used to perform tapping mode AFM on the samples with a silicon tip of 300 kHz frequency. DI Nanoscope software was used to process the raw AFM images. Cyclic voltammetry scans were recorded on a CHI411 instrument from CH Instruments, Inc. UV−vis spectra were recorded with a Varian Cary 6000i UV−vis spectrophotometer with samples prepared in ambient conditions. Ultraviolet photoelectron spectroscopy (UPS) in ambient conditions was performed with a Riken Keiki Co. Ltd. model AC-2 surface analyzer to obtain the ionization potential of the 45 nm organic thin films.

Crystallographic Investigations. Single crystals of the materials were analyzed on a Bruker-Nonius X8 Proteum CCD diffractometer using Cu Kα radiation.

FET Device Fabrication. Top contact devices were made according to a literature procedure.[17] A thermally grown dry silicon dioxide layer (300 nm) with a capacitance per unit area of 1.0×10^{-8} F/cm² functioned as the dielectric, while a heavily n-doped silicon substrate functioned as the gate electrode. The substrates were cleaned by immersion in freshly prepared piranha solution for 45 min. OTS-Y treatment was done by spin-coating a 3 mM solution of octadecyltrimethoxysilane (OTMS) in trichloroethylene on the piranha-cleaned wafer, then placing the substrate in an environment saturated with ammonia vapor for 12 h. The wafers were then sonicated in toluene for 5 min and dried with a nitrogen gun. Octadecyltrichlorosilane (OTS) was vapor deposited by placing the same cleaned wafers in a chamber that had 3−5 drops of OTS. The chamber was then immediately evacuated for 3 min at a vacuum of −27 mmHg, then heated to 150 °C uniformly for 18 h. The vapor-grown OTS (OTS-V) substrates were then annealed at 100 °C for 2 min, then sonicated in toluene and rinsed with dichloromethane and ethanol. For a hydroxyl-free dielectric, a divinyl-tetramethylsiloxane-bis(benzocyclobutene) derivative (BCB) was deposited on a heavily n-doped silicon substrate according to

literature procedures,[14] and a capacitance of 9.09×10^{-9} F/cm² was measured accordingly. Shadow masks with *W/L* of 20 (*W* = 1000 μm, *L* = 50; *W* = 2000 μm, *L* = 100 μm; and *W* = 3000 μm, *L* = 150 μm) were used after the evaporation of the organic semiconductor to deposit the gold drain and source electrodes. The organic semiconductors were deposited at a rate of 0.2−0.3 Å/s under a pressure of 4−6 $\times$ 10⁻⁶ Torr to a final thickness of 45 nm as determined in situ by a quartz crystal monitor. TFT measurements were performed in air or in the nitrogen glovebox using a Keithley 4200 semiconductor parameter analyzer.

Results

We wanted to tune the HOMO and LUMO levels of the tetraceno[2,3-*b*]thiophene[18] conjugated core with different electron-withdrawing substitutions to see if we could lower the LUMO enough to induce n-type behavior under ambient conditions. The lowered LUMOs may stabilize the negative charge carriers and prevent them from being trapped by oxygen or moisture, such that they are stable in ambient, as first demonstrated with hexadecylfluorinated copper phthalocyanine.[19] Also, fluorine-based functionalizations were motivated by reports that naphthalene[20,21] and perylene tetracarboxylic diimide[22−25] (PTCDI)-based molecules with fluoro substituents demonstrate electron transport in OTFTs in air because the perfluoroalkyl chains possess a larger van der Waals radii than alkyl chains, and by doing so, the perfluoroalkyl groups act as a kinetic barrier[20] to limit the diffusion of oxygen into the thin film, preventing electrons from being trapped by molecular oxygen. However, the jury is still out on the role of perfluoroalkyl groups,[26] as others have found that the rate of decay of electron mobility in air is independent of the degree of fluorination. Regardless, making an air-stable n-type OTFT with pentacene derivatives is not trivial, because even a perfluoropentacene[27] TFT is not air-stable. As shown in Scheme 1, we made a few new molecules with varying degrees of fluorination. Previously, we reported on the ambipolar 7,8,9,10-tetrafluoro-5,12-bis(tri-isopropylsilylethynyl)tetraceno[2,3-*b*]thiophene[28] (molecule **13** in Figure 7). Expanding on this, using precursors **a**, **d**[29] and **h**,[30] we functionalized the tetraceno[2,3-*b*]thiophene core at the α position of the thiophene with bromo, fluoro and pentafluorophenyl to give molecules **2**, **10**, **11** and **12** using the Mukaiyama aldol condensation. These molecules were further

(17) Locklin, J.; Roberts, M. E.; Mannsfeld, S. C. B.; Bao, Z. *J. Macromol. Sci., Part C: Polym. Rev.* **2006**, *46*, 79−101.

(18) Tang, M. L.; Okamoto, T.; Bao, Z. N. *J. Am. Chem. Soc.* **2006**, *128*, 16002−16003.

(19) Bao, Z. A.; Lovinger, A. J.; Brown, J. *J. Am. Chem. Soc.* **1998**, *120*, 207−208.

(20) Katz, H. E.; Lovinger, A. J.; Johnson, J.; Kloc, C.; Siegrist, T.; Li, W.; Lin, Y. Y.; Dodabalapur, A. *Nature* **2000**, *404*, 478−481.

(21) See, K. C.; Landis, C.; Sarjeant, A.; Katz, H. E. *Chem. Mater.* **2008**, *20*, 3609−3616.

(22) Jones, B. A.; Facchetti, A.; Wasielewski, M. R.; Marks, T. J. *J. Am. Chem. Soc.* **2007**, *129*, 15259−15278.

(23) Jones, B. A.; Ahrens, M. J.; Yoon, M. H.; Facchetti, A.; Marks, T. J.; Wasielewski, M. R. *Angew. Chem., Int. Ed.* **2004**, *43*, 6363−6366.

(24) Schmidt, R.; Ling, M. M.; Oh, J. H.; Winkler, M.; Konemann, M.; Bao, Z. N.; Wurthner, F. *Adv. Mater.* **2007**, *19*, 3692−3695.

(25) Chen, H. Z.; Ling, M. M.; Mo, X.; Shi, M. M.; Wang, M.; Bao, Z. *Chem. Mater.* **2007**, *19*, 816−824.

(26) Weitz, R. T.; Amsharov, K.; Zschieschang, U.; Villas, E. B.; Goswami, D. K.; Burghard, M.; Dosch, H.; Jansen, M.; Kern, K.; Klauk, H. *J. Am. Chem. Soc.* **2008**, *130*, 4637−4645.

(27) Sakamoto, Y.; Suzuki, T.; Kobayashi, M.; Gao, Y.; Fukai, Y.; Inoue, Y.; Sato, F.; Tokito, S. *J. Am. Chem. Soc.* **2004**, *126*, 8138−8140.

(28) Tang, M. L.; Reichardt, A. D.; Miyaki, N.; Stoltenberg, R. M.; Bao, Z. *J. Am. Chem. Soc.* **2008**, *130*, 6064−6065.

(29) Subramanian, S.; Park, S. K.; Parkin, S. R.; Podzorov, V.; Jackson, T. N.; Anthony, J. E. *J. Am. Chem. Soc.* **2008**, *130*, 2706−2707.

(30) Chen, M. C.; Kim, C.; Chen, S. Y.; Chiang, Y. J.; Chung, M. C.; Facchetti, A.; Marks, T. J. *J. Mater. Chem.* **2008**, *18*, 1029−1036.

Scheme 1. Synthesis of the New Acenes Presented Herein[a]
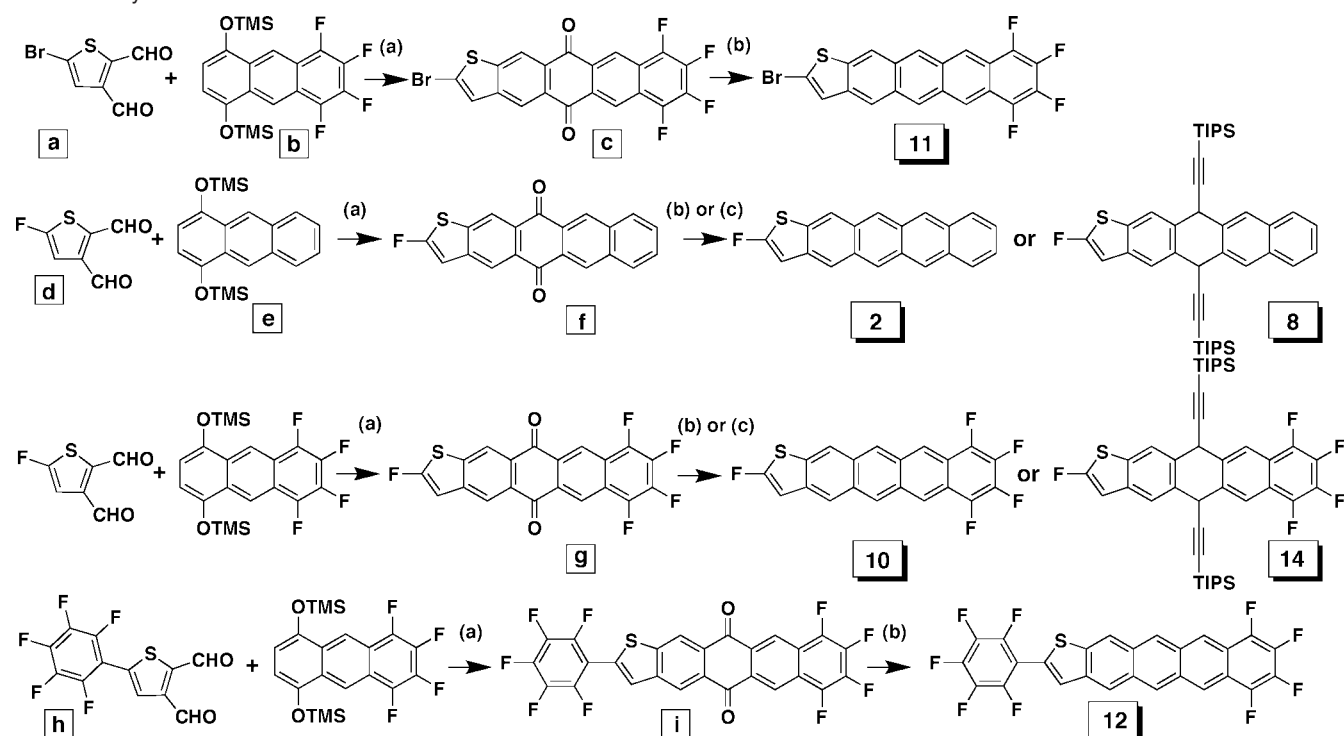
[a] Reagents and conditions: (a) i. tris(pentafluorophenyl)boron, CH$_2$Cl$_2$, RT; ii, CF$_3$CH$_2$OH, reflux, (b) Al, HgCl$_2$, CBr$_4$, CyOH, reflux, (c) i, *n*BuLi, ether, TIPSacetylene, 60°C; ii, SnCl$_2$·H$_2$O, 60 °C.

Table 1. Summary of the HOMO, LUMO and λ_{MAX} in Solution, as Well as the λ_{MAX}, Ionization Potential and Bandgap, E_g, in Thin Film of the Acenes

	solution[a,b]				thin film[c,d,e]		
molecule	LUMO/eV	HOMO/eV	HOMO−LUMO/eV	λ_{MAX} (nm)	E_g/ eV	λ_{MAX} (nm)	ionization potential/eV
7	−3.18	−5.21	2.03	596.1	2.00	602.6	5.12
8	−3.17	−5.25	2.08	579.6	1.92	601.3	5.08
13	−3.38	−5.39	2.01	598.6	1.87	617.0	5.26
14	−3.38	−5.45	2.07	579.6	2.02	587.0	5.45
2	−2.80	−5.15	2.35	515.2	2.03	583.1	5.42
4	−2.90	−5.17	2.27	532.1	1.97	599.4	4.85
9	−3.08	−5.33	2.25	533.2	2.07	582.2	5.76
10	−3.09	−5.39	2.30	516.4	2.04	561.3	5.30
11	−3.11	−5.38	2.27	525.6	2.07	571.3	5.73
12	−3.18	−5.38	2.20	541.3	1.92	597.7	5.81

[a] λ_{MAX} measured in THF. [b] HOMO/LUMO measured by cyclic voltammetry in degassed CH$_2$Cl$_2$ with 0.1 M TBAFPF$_6$ as the electrolyte, with respect to a Fc/Fc$^+$ reference (−4.8 eV to vacuum) added after each measurment. [c] 45 nm thin film made by evaporation under high vacuum. [d] Ionization potential measured in ambient by UPS. [e] E_g, the bandgap, on quartz with the long wavelength absorption edge.

purified by sublimation in a three-zone furnace under high vacuum. Molecules **8** and **14**, being soluble by virtue of possessing two tri-isopropylsilyl (TIPS)-ethynyl groups, were purified by two successive recrystallizations in degassed hexanes, to give purple, needle-shaped crystals. These molecules form a reddish purple solution.

Cyclic voltammetry (CV) was performed with 0.1 M tetrabutylammonium hexafluorophosphate in dichloromethane at room temperature. This, and the UV−vis absorption measurements both in solution and thin film for the new molecules **2**, **8**, **10**, **11**, **12** and **14** are summarized in Table 1. The HOMO/LUMO levels measured by CV are also presented in Figure 1. By comparing these molecules to each other and known

molecules, for example, **7** to **13**, **8** to **14** and **4** to **9**, we can see in Figure 2 that four Fs attached to the terminal benzene ring of the conjugated core lowers the HOMO by approximately 0.20 eV, but the HOMO−LUMO gap remains relatively unchanged. However, the HOMO−LUMO gap increases by 0.05−0.08 eV when the α-H on tetraceno[2,3-*b*]thiophene is replaced by α-F, which can be seen when comparing **7** to **8**, **13** to **14**, **4** to **2** and **9** to **10**. This is mainly due to the HOMO decreasing more than the LUMO, except for the pair **2** and **4**, where the LUMO is closer to vacuum for the fluorinated tetraceno[2,3-*b*]thiophene. As expected, functionalization with the perfluorophenyl moiety does not greatly affect the HOMO−LUMO gap of the molecule, due to the relatively large phenyl−thiophene twist angle; therefore, **12** has a gap of 2.0 eV compared to 1.96 eV for the parent tetraceno[2,3-*b*]thiophene molecule. Table 1 lists the bandgap of 45 nm evaporated thin films, as determined by the absorption edge, and their ionization potential as measured in air by ultraviolet photoelectron spectroscopy (UPS). The ionization potential of the thin film does not show much correlation with HOMO levels measured in solution due to the complications of morphological effects and potential contamination or degradation of the thin films in air.

We made vacuum evaporated, top-contact OTFTs[17] from all the molecules in Table 1 to evaluate their carrier types. The active layer was 45 nm thick, as measured during deposition with a quartz crystal microbalance (QCM). The molecules were evaporated on a 300 nm thermally grown silicon dioxide layer, which served as the dielectric on a heavily n-doped silicon common bottom gate. The SiO$_2$ dielectric was used as is, or modified with a self-assembled monolayer, either octadecyltrichlorosilane (OTS-V) or octadecyltrimethoxysilane (OTMS) in two ways. Octadecyltrimethoxysilane was deposited by spin-coating onto the thermally grown SiO$_2$ substrate (OTS-Y), and octadecyltrichlorosilane by vapor deposition (OTS-V) as out-
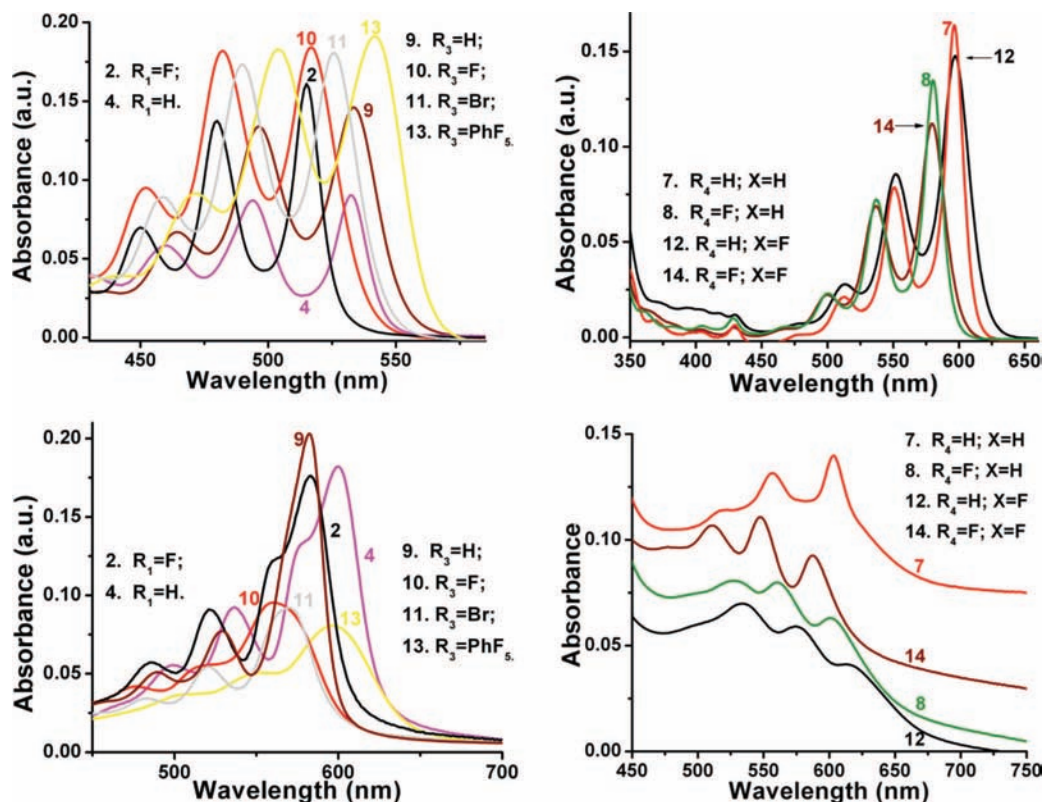
Figure 1. UV−vis of the molecules summarized in Table 1, both in THF (top) and thin film (bottom). The numbering system follows that in Figure 1.
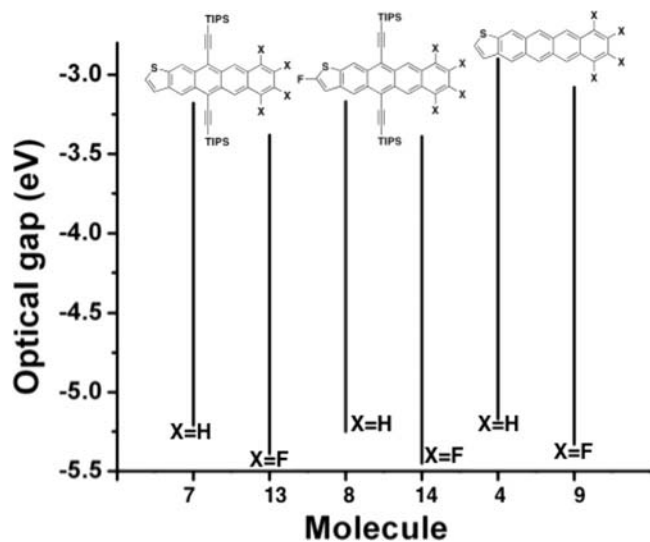

Figure 2. Optical gap of the molecules **7** and **13**, **8** and **14**, **4** and **9** measured by UV−vis in THF. With tetrafluorination at the terminal benzene ring, there is no change in the optical gap, but the energy levels of the molecules decrease by 0.2 eV. The numbering system follows that in Figure 7.

lined in the Experimental Section. Although both kinds of OTS treatment led to the same contact angle, ∼105°, spin-coated OTS-Y is a crystalline and densely packed monolayer, whereas the vapor-deposited OTS-V is disordered.[31] The substrate temperature was held at RT and 60 °C, and sometimes at 70 or 90 °C if the mobility was high and the material seemed to merit further investigation.

The results from OTFT current−voltage measurements are shown in Tables 2 and 3. Molecules **7** and **13** were previously reported, where **7** had hole mobilities >1 cm^2 V^{-1} s^{-1} and **13** had both hole and electron mobilities >0.1 cm^2 V^{-1} s^{-1}. Similar to **13**, molecules **8** and **14** displayed ambipolar behavior. Only **14** showed high and balanced mobilities >0.1 cm^2 V^{-1} s^{-1}, while **8** had good hole current, but electron mobilities were an order of magnitude lower. We think this is related to the relatively higher LUMO of **8**, which represents a larger barrier to electron injection from gold. Both **8** and **14** exhibit the two-dimensional (2D) brick-layer structure that is characteristic of 6,13-TIPS-ethynylpentacene[7] type molecules, as shown in Figure 3. The distance between π−π stacks is 3.26 Å and 3.37 Å for molecules **8** and **14** in single crystals grown from solution. This kind of close packing[32] was used to explain the high mobilities measured for this family of molecules.[33] Interestingly, on both vapor and spin-coated OTS, the hole mobilities and the morphology by atomic force microscopy (AFM) were about the same, but vapor-treated OTS did not give electron transport for any of the molecules in Figure 7. Figure 4 shows AFM images of thin films of molecule **8**, which greatly resemble the AFM of **14**, shown in the Supporting Information. Thin films grown at substrate temperatures, T_D of RT, 60 and 90 °C are shown. At RT and 60 °C, on OTS/SiO$_2$ surfaces, grains of about 0.5 μm can be seen for both **8** and **14**, with a film thickness that is on the same order as the QCM measured thickness. However, at a 90 °C substrate temperature, faceted grains and more 3D growth is seen for **8**. Some of these faceted grains are observed for **14**

(31) Virkar, A. A.; Mannsfeld, S. C. B.; Oh, J. H.; Toney, M. F.; Tan, Y. H.; Liu, G. Y.; Scott, J. C.; Miller, R.; Bao, Z. *Adv. Funct. Mater.* **2009**. In press.

(32) Anthony, J. E.; Brooks, J. S.; Eaton, D. L.; Parkin, S. R. *J. Am. Chem. Soc.* **2001**, *123*, 9482–9483.

(33) Sheraw, C. D.; Jackson, T. N.; Eaton, D. L.; Anthony, J. E. *Adv. Mater.* **2003**, *15*, 2009–2011.

Table 2. Average OFET Mobilities, μ, and Their Standard Deviations, with the On/Off Ratios and Threshold Voltages, V_T, on 45 nm Top Contact Devices with Gold Electrodes, $W/L = 20$, $L = 100\ \mu$m, Measured in Air and in Nitrogen; OTS Reported Here Was Spin-Coated OTS-Y

		environment	air		nitrogen	
		substrate	SiO₂	OTS/SiO₂	OTS/SiO₂	
molecule	T_D/°C	carrier	hole	hole	hole	electron
8	RT	μ (cm² V⁻¹ s⁻¹)	0.0132 ± 0.007	0.274 ± 0.03	0.241 ± 0.02	(2.52 ± 1)E-3
		on/off	3E+06	4E+02	3E+06	2E+03
		V_T (V)	−20	−30	+20	+160
	60	μ (cm² V⁻¹ s⁻¹)	(5.21 ± 0.6)E-4	0.141 ± 0.02	0.233 ± 0.02	0.0393 ± 0.02
		on/off	2E+04	1E+07	3E+03	1E+05
		V_T (V)	−50	+30	+20	+80
	90	μ (cm² V⁻¹ s⁻¹)	no TFT	0.111 ± 0.03	0.0715 ± 0.02	0.0359 ± 0.02
		on/off		6E+05	8E+02	6E+04
		V_T (V)		+40	+40	+120
14	RT	μ (cm² V⁻¹ s⁻¹)	(9.83 ± 3)E-4	0.0672 ± 0.03	0.157 ± 0.07	0.0376 ± 0.007
		on/off	3E+05	7E+06	4E+04	1E+05
		V_T (V)	−50	−20	+10	+80
	60	μ (cm² V⁻¹ s⁻¹)	(9.16 ± 2)E-5	0.154 ± 0.1	0.293 ± 0.09	0.104 ± 0.02
		on/off	4E+03	5E+06	1E+04	9E+05
		V_T (V)	−40	−5	+10	+90

Table 3. Average p-Channel OFET Mobilities of **2**, μ, the Standard Deviation, On/Off Ratios and Threshold Voltages, V_T, on 45 nm Top Contact Devices with Gold Electrodes, $W/L = 20$, $L = 50\ \mu$m in Air; No n-Channel Field-Effect Transistor Was Observed for **2** Even in Dry Nitrogen

T_D/°C		SiO₂	OTS/SiO₂
RT	μ (cm² V⁻¹ s⁻¹)	0.0507 ± 0.01	0.0546 ± 0.03
	on/off	1E+03	5E+07
	V_T (V)	>+60	−20
60	μ (cm² V⁻¹ s⁻¹)	0.0393 ± 0.02	0.298 ± 0.06
	on/off	2E+02	2E+07
	V_T (V)	>+60	+10
70	μ (cm² V⁻¹ s⁻¹)	0.0325 ± 0.008	0.269 ± 0.05
	on/off	1E+03	5E+07
	V_T (V)	>+60	−20

at 60 °C also. For both molecules, the best OTFT performance occurs when T_D = 60 °C.

Of all the new linear molecules made, only **2**, 2-fluoro-tetraceno[2,3-*b*]thiophene, showed respectable mobility, with an average mobility of 0.3 cm² V⁻¹ s⁻¹ on OTS modified substrates held at 60 °C, and a maximum mobility of 0.42 cm² V⁻¹ s⁻¹. The OTFT data for this molecule is shown in Table 3. There was no significant increase in mobility when the substrate temperature was increased to 70 °C. AFM of this molecule (Figure 5) shows layer by layer growth, with grains larger than 1 μm. Figure 5 shows a screw dislocation (top, middle AFM at T_D = 60 °C on OTS/SiO₂), which has been reported before in well-ordered, high-mobility molecules like pentacene.[34] **2** did not display any electron transport, even in the glovebox. Typical OTFT output and transfer curves are shown in Figure 6.

Molecules **10**, **11** and **12**, the tetraceno[2,3-*b*]thiophene molecules tetrafluorinated on the terminal benzene ring, did not give high mobility OTFTs. Although ambipolar OTFT behavior was observed for **10** and **12** (shown in the Supporting Information), the on currents were low, and the resulting mobilities were <10⁻⁴ cm² V⁻¹ s⁻¹. Unlike the previous molecules where all devices worked uniformly, devices from these molecules did not show a transistor gating effect more than 50% of the time. Examination of the AFM images of molecules **10**, **11** and **12** shows two kinds of morphology: highly 3D grains on the order

(34) Nickel, B.; Barabash, R.; Ruiz, R.; Koch, N.; Kahn, A.; Feldman, L. C.; Haglund, R. F.; Scoles, G. *Phys. Rev. B* **2004**, *70*, 125401.

of a few 100 nm, especially at T_D = 60°, far exceeding the targeted QCM thickness of 45 nm, and elongated grains a few hundred nanometers in length on the order of 20−30 nm tall. Large gaps between grains are clearly visible for the 3D grains. Devices with elongated grains did not display any mobility either (see Supporting Information). These molecules behaved like the previously reported tetrafluorinated parent molecule, **9**.[28] Further analysis is being done to obtain the packing of these thin films, to determine how tetrafluorination at the terminal fused benzene ring affects the packing of the molecules in thin film, and hence their mobility.

X-ray diffraction of these thin films gives the out-of-plane *d*-spacing. The plots of the raw data and values of the *d*-spacing are in the Supporting Information. For the molecules with high mobility, **2**, **8** and **14**, the intensity of the peaks and the narrowness of the full-width-at-half-maximum (fwhm) correlate with the measured mobility, with films that had higher mobility having more intense peaks with a smaller fwhm. For the molecules with low mobility, either the film appeared amorphous, or more than one phase seemed to coexist. For example, no peaks were seen for **11** (which did not show any field-effect transistor) while **10** and **12** showed peaks close together that indicate there may be more than one phase. This might explain why these molecules did not give OTFTs with high mobility.

Discussion

We plotted 19 molecules in Figure 7, with the HOMO plotted on the *y*-axis on the right, represented in red diamonds, and the LUMO on the left, represented in blue squares. The molecules are plotted from left to right in order of the decreasing LUMO (further away from the vacuum). All these devices were 45 nm thick thin films in the top-contact geometry with gold electrodes and spin-coated OTS/SiO₂.

The shaded area in Figure 7 includes molecules that gave ambipolar behavior in nitrogen. To the left of this shaded area are molecules that only exhibited hole transport, while to the right of this shaded box is perfluoropentacene, made by the Suzuki group.[27] We synthesized molecules **16** and **18** in Figure 7 according to Anthony's literature procedures.[35] They are 6,13-TIPS-ethynyl-pentacene with tetrafluoro and octafluoro substitutions on the sp² hydrogens of the terminal benzene rings, respectively. It was previously reported that both these molecules gave hole mobilities of less than 0.025
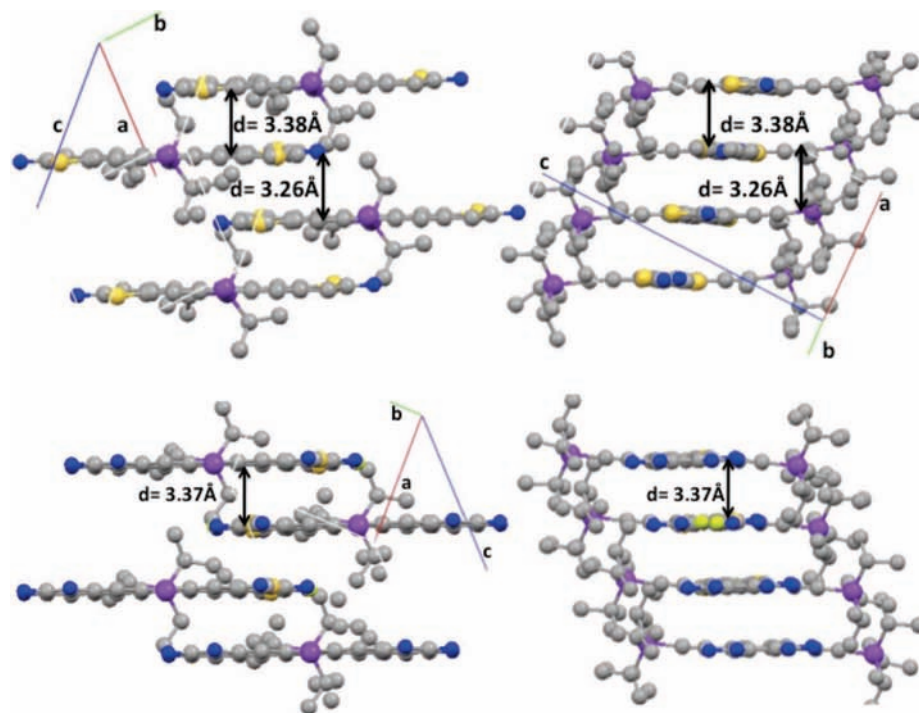
Figure 3. Solution-grown single-crystal structures of **8** (top) and **14** (bottom) that show their 2D bricklayer structure. On left, the tri-isopropylsilylethynyl groups in the front have been removed for clarity. Hydrogen atoms have been omitted for clarity as well, while blue spheres depict F atoms, yellow spheres S atoms, purple spheres Si, and gray spheres C.
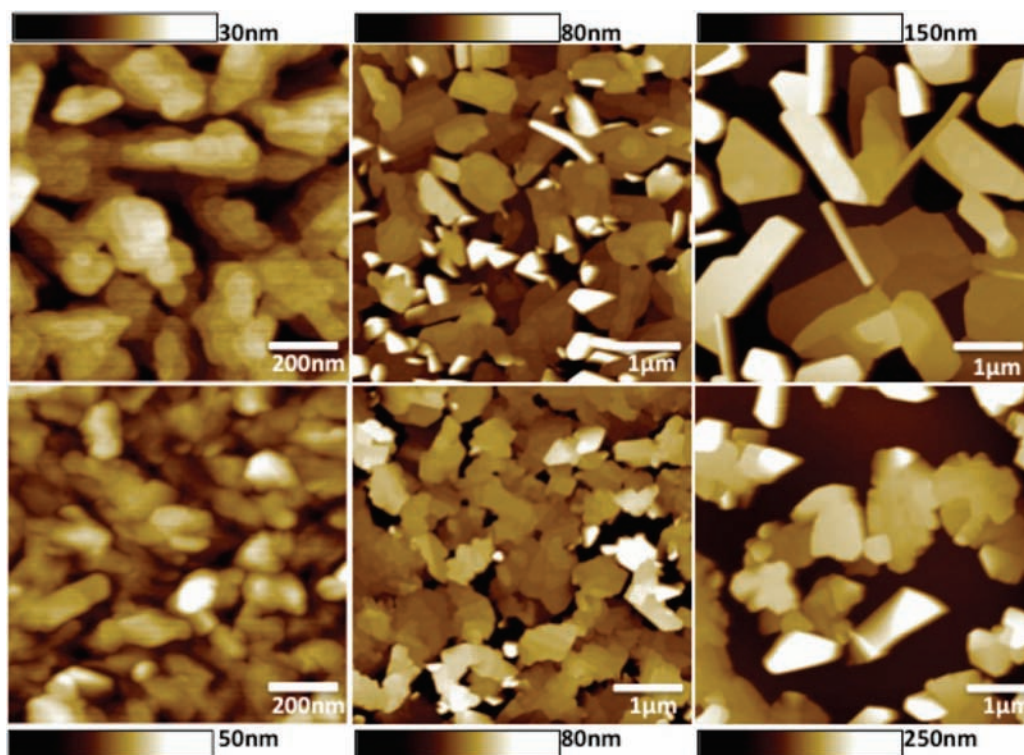

Figure 4. AFM images of **8** at a substrate temperate, T_D, of RT (left), 60 °C (middle) and 90 °C (right); on OTS/SiO₂ (top) and on SiO₂ (bottom).

$cm^2 V^{-1} s^{-1}$ on SiO_2, but no electron transport.[35] This is in line with the knowledge that SiOH silanol groups are reduced in the presence of a positive gate voltage to give negatively charged, bridged $Si-O^-$ that are electrochemically trapped at the semiconductor−dielectric interface.[14] These anions effectively screen the electric field across the dielectric induced by the gate voltage and shift the threshold voltage

of the device outside the measurement window. With our crystalline spin-coated OTS that encapsulate the SiOH traps, both these molecules displayed good ambipolar behavior when characterized in the glovebox.

As mentioned before, OTS made by the vapor treatment of octadecyltrichlorosilane did not give any ambipolar devices. It has been shown that the reaction of alkyltrichlorosilanes with
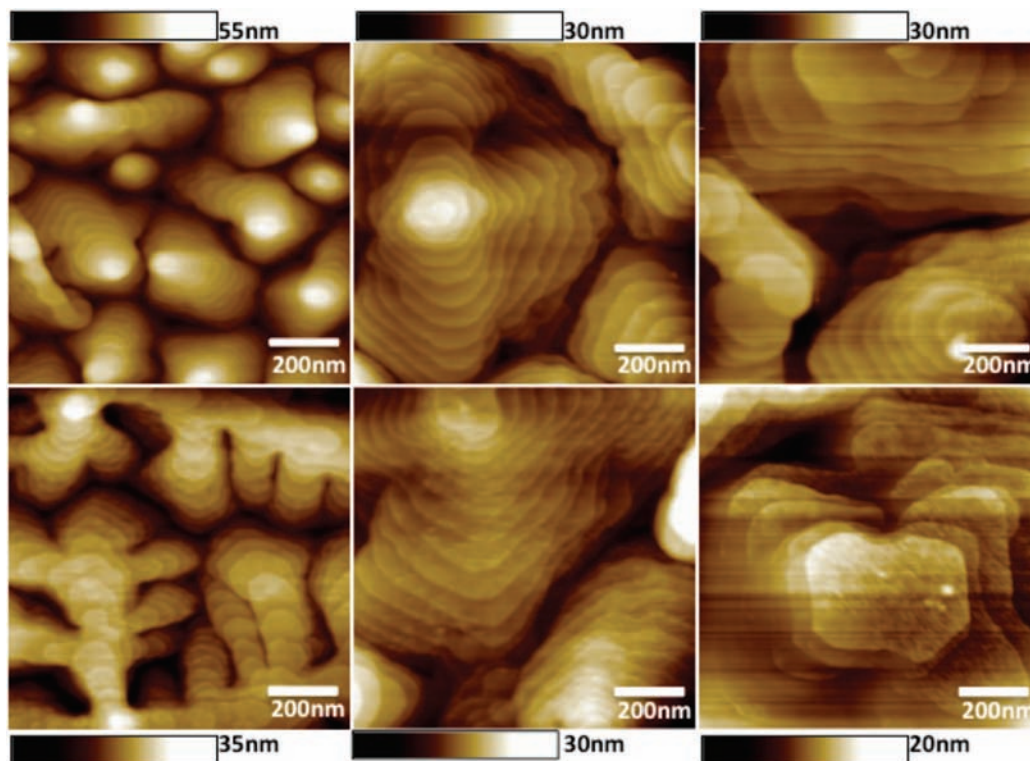
Figure 5. AFM images of **2** at a substrate temperate, T_D, of RT (left), 60 °C (middle) and 70 °C (right); on OTS/SiO$_2$ (top) and on SiO$_2$ (bottom).
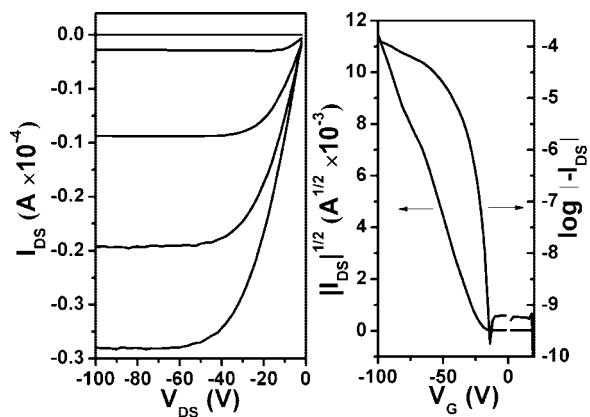

Figure 6. Typical OTFT transfer and output curves of **2** at a substrate temperature, T_D = 60 °C on OTS/SiO$_2$, with Au electrodes, W/L = 20, L = 50 μm measured in air.

silanol groups is not quantitative, leaving unreacted Si-OH groups on the surface.[36] To have eliminated electron transport, the density of these Si-OH groups on our vapor-grown OTS surface in addition to the deep traps within the OSC layer may be at least on the order of the charge carrier concentration, approximately 10^{12}–10^{13} cm^{-2} at around a 100 V gate voltage for a 300 nm oxide dielectric. Previously, others used C10 and C18 alkyltrichlorosilane self-assembled monolayers (SAMs) deposited from solution as a tunneling barrier for electrons to the traps at the Si-OH interface.[14] This resulted in the threshold voltage shifting toward more and more positive values with each successive measurement. In our case, we did not observe any electron current even in the first sweep of the transfer curve

with a positive gate voltage for vapor-treated OTS. We note that the same contact angle of ~105° was obtained for both spin-coated and vapor-grown OTS. However, our spin-coated OTS was shown to have a higher surface coverage than the vapor-grown OTS.[31]

Figure 7 clearly shows the onset of electron and hole injection with respect to the molecular HOMO and LUMO levels. With many molecules having energy levels quite close to each other, we can see that with gold electrodes, electron injection commences when the LUMO < −3.15 eV, and that once the HOMO drops below −5.6 eV, hole injection is no longer favorable. Acenes that have their HOMOs less than 5.6 eV and LUMOs more than 3.15 eV from vacuum respectively display ambipolar transport. Pentacene,[37] which fits between molecules **12** and **13** in the shaded area in Figure 7 in terms of HOMO and LUMO levels, has already demonstrated ambipolar transport as shown by Singh et al. on a poly(vinylalcohol) (PVA) dielectric. PVA is less polarizable than poly(vinylphenol) (PVP), with dielectric constants of 3.9 and 8, respectively. Singh[37] and co-workers were not able to measure n-channel pentacene OTFTs on PVP, while Chua et al.[14] did not observe any electron transport on relatively acidic polymeric dielectrics such as PVP or polyimides. With Au electrodes, electron transport was only reported for F8T2 (poly(9,9-dioctylfluorene-*alt*-bithiophene). F8T2 has a LUMO of 3.1 eV, which is the threshold upon which we observe electron injection from gold for our molecules. With calcium electrodes and a divinyltetramethylsiloxane-bis(benzocyclobutene) derivative (BCB) dielectric, they saw n-channel devices for all the eight polymers that had LUMOs range from 2.4 eV to 3.3 eV. Out of these eight polymers, two did not transport holes with Au electrodes. The HOMO levels of these

(35) Swartz, C. R.; Parkin, S. R.; Bullock, J. E.; Anthony, J. E.; Mayer, A. C.; Malliaras, G. G. *Org. Lett.* **2005**, *7*, 3163–3166.

(36) Angst, D. L.; Simmons, G. W. *Langmuir* **1991**, *7*, 2236–2242.

(37) Singh, T. B.; Meghdadi, T.; Gunes, S.; Marjanovic, N.; Horowitz, G.; Lang, P.; Bauer, S.; Sariciftci, N. S. *Adv. Mater.* **2005**, *17*, 2315–2320.
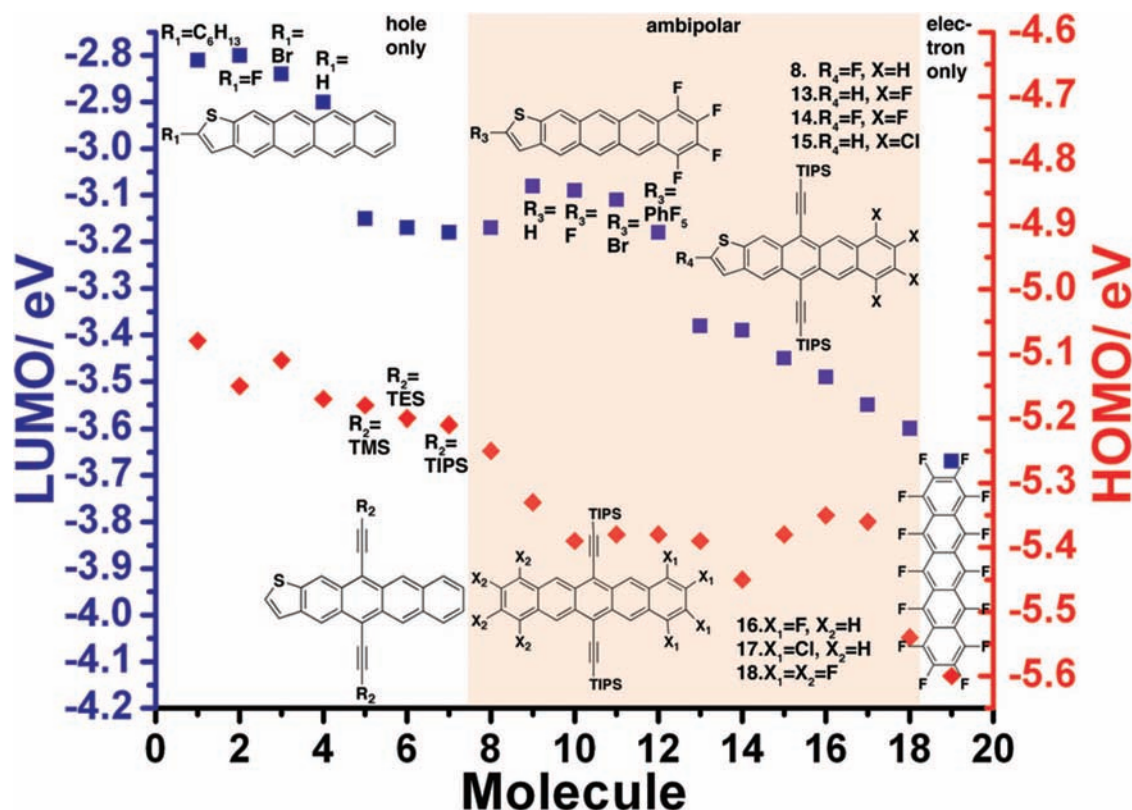
Figure 7. Plot of 19 acenes with a range of HOMO (right *y*-axis, red diamonds) and LUMO (left *y*-axis, blue squares) levels. The charge carrier type was measured using the top-contact field-effect transistor geometry, with gold electrodes on OTS-Y modified surfaces. The devices vary from those that display hole-only transport, to ambipolar, to electron-only transport according to frontier molecular energy levels. Molecules **6** and **11** do not show OFET characteristics due to discontinuous films formed when evaporated under high vacuum. They are included because their energies fall in the indicated range, and therefore their carrier types in TFT geometry are predicted for a film with better morphology.

polymers are <-5.4 eV (this being the HOMO level of CN-PPV: poly(2,5-dihexoxy-α,α'-dicyano-*p*-xylylidene-*alt*-2,5-di-hexoxy-*p*-xylylidene), close to the -5.6 eV in our observations. It is interesting to note that with Au electrodes, ambipolar field-effect transistors have been measured for single crystals of Cu- and Fe-phthalocyanines[38] (hole mobility 0.3 cm^2 V^{-1} s^{-1}; electron mobility 0.03 cm^2 V^{-1} s^{-1}) but not for thin films of **FePc** (which are hole-only devices), while an electron mobility of $<10^{-5}$cm^2 V^{-1} s^{-1} was measured for a thin film of **CuPc**.[39] This suggests that structural disorder in the thin film also limits the observation of charge transport of a certain carrier type, in this case electrons. This might explain why CN-PPV, being inherently more disordered than the polycrystalline small molecules reported here, does not display hole transport with Au electrodes despite having a HOMO of -5.4 eV which is more positive than the threshold for hole injection in this work, that is -5.6 eV.

We note that molecules **9**–**12** have a LUMO slightly closer to vacuum compared to molecules **5**–**7**, and since **9**–**12** are ambipolar, **5**–**7** should be as well. However, this is not the case, **5**–**7** transport only holes. **9**–**12** are the linear tetrafluorinated tetraceno[2,3-*b*]thiophene molecules, while **5**–**7** are trialkylsi-lylethynyl functionalized tetraceno[2,3-*b*]thiophene molecules, which do not have any fluorines attached. While electron injection into thin films of **5**–**7** is possible by virtue of the

position of their LUMO levels, electron transport may be inhibited in these molecules, perhaps due to deep traps within the thin film. To test this hypothesis, we deposited molecule **7** on the BCB dielectric[14] that would unequivocally eliminate all hydroxyl groups on the surface of the substrate, and made top-contact transistors with gold electrodes. In a dry nitrogen environment, no electron transport was measured when a positive gate voltage was applied, while the hole mobility was an average of 0.26 cm^2 V^{-1} s^{-1} (on/off ratio $>10^6$ and threshold voltage $= 10$ V, as summarized in the Supporting Information). Thus, we attribute the lack of electron transport for molecules **5**–**7** to structural factors within the thin film because the BCB dielectric enables us to rule out the role of interfacial electron traps in inhibiting electron transport.

The previous work and ours illustrate the large mismatch in the workfunction of clean polycrystalline Au (-5.3 eV) compared to the barriers for charge injection for holes ($\Delta_h = 0.5$ eV) and electrons ($\Delta_e = 2.0$ eV). Chua and co-workers postulate that there may be an interface dipole that lowers the barrier for electron injection. Experimental evidence for such an interface dipole,[40] which is different for clean and contaminated Au, has been shown by the Kahn group using ultraviolet photoemission spectroscopy (UPS) and current–voltage measurements, with the hole transporting material *N*,*N*′-diphenyl-*N*,*N*′-bis (1-naphthyl)-1,1′-biphenyl-4,4′-diamine (α-NPD). The nature of the interface dipole is not well understood, for example Grobosch and Knupfer[41] suggested from their photoemission

(38) de Boer, R. W. I.; Stassen, A. F.; Craciun, M. F.; Mulder, C. L.; Molinari, A.; Rogge, S.; Morpurgo, A. F. *Appl. Phys. Lett.* **2005**, *86*, 262109.

(39) Opitz, A.; Kraus, M.; Bronner, M.; Wagner, J.; Brutting, W. *New J. Phys.* **2008**, *10*, 065006.

(40) Wan, A.; Hwang, J.; Amy, F.; Kahn, A. *Org. Electron.* **2005**, *6*, 47–54.

studies that the injection barrier, Φ_B, was virtually independent of the metal electrode used when the substrate was contaminated by ambient species. Capelli[42] and co-workers saw that their ambipolar OLET's performance had marginal dependence on the Fermi energy of their contacts, which were exposed to atmosphere during device fabrication. Kahn and co-workers measured a workfunction of as low as −4.7 eV for gold exposed to ambient compared to −5.4 eV for 'clean' gold deposited in UHV. Grobosch et al. observed a workfunction of −5.2 eV for 'clean' gold, and −4.3 eV for contaminated gold. Our devices certainly used contaminated Au with the lower workfunction (since they are exposed to ambient prior to gold deposition), which will decrease the barrier for electron injection. We predict that the observations in Figure 7 are generic for this class of materials using the device structure presented. With a low workfunction metal electrode, molecules with higher LUMO may show electron-transporting behavior. However, the observed trend may be complicated by the high reactivity of low workfunction metals.

It should be kept in mind that while the HOMO/LUMO values reported here and in the paper by the Cambridge group are measured by cyclic voltammetry, it is the energy levels of the thin films that are more relevant to charge injection. Surprisingly, the ionization potentials given by our UPS measurements do not at all correlate with the HOMO levels measured by CV. Typically, UPS is done in ultrahigh vacuum (UHV) on a conductive substrate, while our measurements were done in ambient on device wafers which include a thick oxide. There might have been some radiation damage to our molecules during the measurement, as observed when doing UPS with sexithiophene in UHV.[43] Thompson and Forrest[44] have found a linear relationship between HOMO levels measured by UPS and that measured by CV. However, their simple electrostatic model is based on spherical molecules with a fixed dipole, overlooking metal workfunction, the shape of molecular frontier orbitals, the effect of the electrolyte, and of solvation. They point out that nonspherical molecular shapes, like the linear acenes presented in here, would require the consideration of higher order multipoles and the orientation of the molecule with respect to the conductor. Diffraction based techniques reveal that these acenes have a preferred orientation to the substrate surface. The linear molecules pack with their long axis almost perpendicular to the substrate (like pentacene), while the tri-isopropylsilylethynyl functionalized molecules pack with their long axis (the conjugated core) parallel to the substrate. All of the above factors might explain why our UPS measurements do not correlate with the HOMO levels measured by cyclic voltammetry.

The mobility of these ambipolar acenes depends on the packing of the molecules in thin film, so molecules 9−12, the tetrafluorinated linear tetraceno[2,3-b]thiophenes, have mobilities $<10^{-4}$ cm^2 V^{-1} s^{-1}, while molecules 8, 13−18 have both hole and electron mobilities mostly >0.1 cm^2 V^{-1} s^{-1} (up to 0.6 cm^2 V^{-1} s^{-1}). While the reason for the poor performance of 9,10 and 11 is attributed to their 3D grain morphology, it is not clear

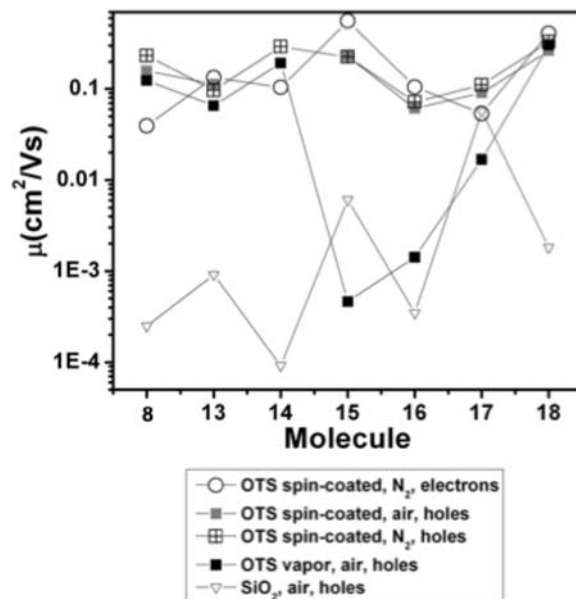**Figure 8.** The hole and electron mobility of molecules 8, 13−18 for different surfaces at optimized device conditions. For 8, 14 and 17, that is $T_D = 60$ °C, for 13 and 16, $T_D = $ RT; and for 15, $T_D = 70$ °C. All the channel lengths were 100 μm, $W/L = 20$. No electron mobility was measured in air or on SiO$_2$ or vapor-grown OTS.

why 12 does not have good mobility despite the AFM showing grains that are relatively 2D on the order of micrometers. These elongated grains are reminiscent of PTCDI based molecules.[22] We're investigating the packing of this series of molecules in order to explain their different behavior in charge transport characteristics. With regards to all the tri-isopropylsilyl acetylene functionalized acenes, 8, 13−18, a high mobility is expected due to their 2D brick-layer π-stacked structure in the single crystal phase. On rare occasions do they have a mobility on the order of 10^{-2} cm^2 V^{-1} s^{-1}, for example 8 has an average hole and electron mobility of 0.241 cm^2 V^{-1} s^{-1} and 0.0359 cm^2 V^{-1} s^{-1} respectively. The relatively low electron mobility might be due to the fact that its LUMO is relatively high, thus there is a higher energetic barrier to electron injection from gold. In addition, the electrons, being relatively high in energy, are more easily trapped by defects and impurities. As can be seen in Figure 8, the hole mobilities on spin-coated OTS do not vary much inside and outside the glovebox. This implies that ambient species are not traps for holes. In general, hole mobility is lower on vapor-grown OTS, and even lower on bare SiO$_2$. This is not surprising considering mobility is influenced by the morphology of the thin film, which depends on the nature of the dielectric and its surface energy.

To conclude, we have correlated the molecular HOMO and LUMO levels for acene organic semiconductors measured in solution to charge carrier type in top-contact OTFTs with gold electrodes and OTS treated substrates. Though this relationship has long been expounded qualitatively before, this is the first systematic study that draws extensive experimental evidence from 20 molecules. These 20 acenes establish that it is energetically favorable for holes to be injected into the HOMO if it is more positive than −5.6 eV; while electron injection into the LUMO commences when it is more negative than −3.15 eV. However, structural disorder or deep traps within the thin film may inhibit the observation of ambipolar behavior. We predict that this kind of empirical trend exists for a given combination of molecular family, electrode and dielectric. More

(41) Grobosch, M.; Knupfer, M. *Adv. Mater.* **2007**, *19*, 754–756.
(42) Capelli, R.; Dinelli, F.; Toffanin, S.; Todescato, F.; Murgia, M.; Muccini, M.; Facchetti, A.; Marks, T. J. *J. Phys. Chem. C* **2008**, *112*, 12993–12999.
(43) Koch, N.; Pop, D.; Weber, R. L.; Bowering, N.; Winter, B.; Wick, M.; Leising, G.; Hertel, I. V.; Braun, W. *Thin Solid Films* **2001**, *391*, 81–87.
(44) D'Andrade, B. W.; Datta, S.; Forrest, S. R.; Djurovich, P.; Polikarpov, E.; Thompson, M. E. *Org. Electron.* **2005**, *6*, 11–20.

such studies revealing similar trends will facilitate the development of computational methods that will help in the rational design of organic semiconductors.

Supporting Information Available: Complete reference 8, crystallographic information files (CIF), synthetic details, plots of XRD OOP measurements with a summary of the *d*-spacings, OTFT current−voltage curves and AFM of molecules **10−12**. This material is available free of charge via the Internet at http://pubs.acs.org.

JA809659B